Hindawi
Mathematical Problems in Engineering
Volume 2019, Article ID 6476037, 11 pages
https://doi.org/10.1155/2019/6476037

Research Article

Anti-Defect Design for Mechanical Elements under Severe Condition Based on a Half-Real Defect Model

Xinyue Zhao, Hongyuan Wang, Jiaomei Yin, and Zaixing He

State Key Lab of Fluid Power and Mechatronic Systems, School of Mechanical Engineering, Zhejiang University, China

Correspondence should be addressed to Zaixing He; zaixinghe@zju.edu.cn

Received 6 November 2018; Revised 16 February 2019; Accepted 6 March 2019; Published 20 March 2019

Guest Editor: Sutasn Thipprakmas

For mechanical elements running under severe working condition, there inevitably exist some small defects caused during working. The weak area, which is sensitive to defects, of the structure is more vulnerable, resulting in early damage during service. This paper describes a novel anti-defect design method for optimizing structure to enhance the reliability of vulnerable areas. First, a half-real defect model derived from the real defect is developed to model the geometrical characteristics of defects. Then, the damage degrees of model parameters are identified by Sobol's sensitivity method and the vulnerable area can be labeled according to the damage degree. Finally, we take the vulnerable area as the object of anti-defect optimization for structure and the optimization variables are selected tendentiously based on parameters with larger damage degrees. The multiobjective particle swarm algorithm is then employed to find the optimal distribution of the variables in order to improve the safety of the sensitive area of structure. We take the impeller blade as the research subject to verify the validity of the proposed method. Analysis results showed that the proposed method can increase the structure strength and delay the damage of the mechanical elements.

1. Introduction

Structure optimization plays an important role in ensuring the reliability of mechanical equipment. Nowadays, more and more researchers have been devoted to this field. Generally, the improvement of structure involves size optimization, shape optimization, and performance optimization. Ananthasuresh [1] first extended the techniques of topological optimization for structure to the design of compliant mechanism. He proposed three models to describe the design problem of compliant mechanism. Zhu et al. [2] used a level set method with distance-suppression scheme for structural topology and shape optimization. Xia et al. [3] used a level set based method to optimize the configuration of piezoresistive sensors. Han et al. [4] investigated the flutter of a compressor blade. They analyzed the influence of clearance parameter, bending stiffness, and torsion on the flutter characteristics of the blade. Fei et al. [5] studied the radial deformation of the turbine blade. Based on ERSM and IDM methods, they proposed an approach and a model for the dynamic reliability optimal design of complex motorial structure and dynamic systems. Staino and Basu [6] proposed a multimodal mathematical model with variable rotor speed for wind turbine blades and studied the impact of blade rotor speed variation on the edgewise vibration. Li et al. [7] studied the flapwise dynamic response of a rotating wind turbine blade subjected to unsteady aerodynamic loads in superharmonic resonance. They used a multiple-scale method to get analytical solutions for positive aerodynamic dampings having the same order with dynamic displacements. Hong et al. [8] studied the optimal design of engine cylinder head by the topology optimization, which would be helpful to structure design.

In recent years, the intelligent optimization algorithm has become a new hot subject for the improvement of structure. Islam et al. [9] presented a numerical optimization framework based on coupled Genetic Algorithm and Finite Element Analysis for optimizing the arc welding process. Liu et al. [10] used a microgenetic algorithm to calculate the optimal solution of variables for improving the efficiency of the mixed-flow pump. Song et al. [11] used intelligent CAD and Finite Element Analysis to design turbine blade fir-tree root. They examined the effects of critical geometric features on stress distribution at the interface between the blade and

disk. Chen et al. [12] developed a procedure combining Finite Element Analysis and particle swarm algorithm to optimize composite structures of the wind turbine blades.

Most of the above optimization methods are built on nondamage mechanical elements. For mechanical elements running under the circumstance of heavy loads, corrosion, and other bad factors, there inevitably exist small defects due to the severe working condition. Different structures have their own weak areas. Once the defects grow in these areas, damage will be caused immediately, which may result in serious accidents [13, 14] . Without considering defects, these methods could not improve structure through targeted optimization.

To overcome this problem, in this paper, a novel anti-defect optimization method based on a half-real defect model and Sobol's sensitivity is proposed to enhance structure for defect resisting. First a parameterized model for defects based on the image is introduced to identify the essential features of the real defects. With this model, the damage state of the structure is simulated by changing the model parameters. Then based on Sobol's sensitivity, the weak area which is sensitive to defects is found according to the influence levels of model parameters. Finally the structure can be improved by optimizing the defect-sensitive area with the SVM (Support Vector Machine) [15] and the PSO (particle swarm optimization) methods [16]. SVM is a kind of supervised learning model used for classification and regression analysis. In our approach, the final prediction model of optimization variables and optimization goal are formed based on SVM. PSO is a computational method that optimizes a problem by iteratively trying to improve a candidate solution with regard to a given measure of quality. The PSO method is adopted finally to determine the optimal solution set.

The contributions of the paper are summarized as follows.

(1) A Half-Real Defect Model Is Built to Improve the Strength of Mechanical Elements. So far, most of the studies focus on the nondamage structure optimization. They ignore the influence of defects. Even if a few of them consider defects, they only simplify the defect to an ellipse or a line, which may lose some effective information and could not describe the real situation [17, 18]. On the other hand, it is not feasible to express all properties of the real defect. From this point, in this paper, we proposed a half-real defect model based on the real defect shape information to simulate the injured components.

(2) Sobol's Sensitive Method Is Adopted to Avoid the Blindness of Choosing Optimization Variables. The traditional optimization variables are usually defined according to all the related structural parameters. In this paper, based on Sobol's sensitive method, the vulnerable area of the structure is determined based on the damage degree of the model parameters. The defect-sensitive parameters are chosen as optimization variables selectively. This process can simplify the optimization parameters, making it more specific and more targeted.

This paper is organized as follows. In Section 2, a half-real defect model is developed. In Section 3, Sobol's sensitivity method is adopted based on the model and the PSO optimization method is introduced. In Section 4, an example with the impeller blade is discussed in detail. Finally, conclusions are summarized in Section 5.

2. The Half-Real Defect Model

Most of the defect models simplify the crack to the ellipse or the line shapes, which may lose some effective information and could not describe the real situation. But on the other hand, the geometric characteristics of the real defects in the components are really complicated. Most cracks have highly irregular shapes and very small sizes. Thus, it is not feasible to express all properties of the real defect. Since it is difficult to build the real defect model, a half-real defect model based on the shape information of the crack is proposed in this paper.

2.1. Real Defect Extraction. The real geometric shape of the defect can be obtained completely using the image processing methods [19–21] . It is proved that the image processing methods have the advantage of convenience and accuracy in the research of obtaining geometric features of defects.

The crack is the most common defect of the mechanical components. A typical crack usually involves the crack length, the crack width, the crack depth, and the crack propagation. Therefore, the selected crack image which is used for building the defect model should have these typical representative characteristics.

In this paper, the typical crack image which is shown in Figure 1(a) is used. There are three segments of the crack, and we picked the rightmost one which has the obvious shape characteristic and its curve is relatively clear. Since a parameterized step will be adopted later, the differences of crack images do not influence the final modeling greatly.

To extract the real defect, the original image is first converted to the binary one by suitable threshold (Figure 1(b)). Since the binary operation can produce cavities and noises, morphological processing methods are processed to make the defect more compact and reduce small noises in the background (Figure 1(c)). Then, the cleaning processing is applied to remove the regions of no-interests (Figure 1(d)). Finally, the crack boundary (Figure 1(e)) and the crack skeleton (Figure 1(f)) are acquired.

2.2. Parameterization of the Defect Model. The extracted real defects are parameterized which can express the geometrical characteristic of the defects well and are more universal in some respects. This process contains two aspects: the model simplification and the model parameterization.

2.2.1. Model Simplification. To parameterize the model, we have to simplify the extracted defects at first. Crack edges are not straight and are usually shown as irregular lines. For this reason, a geometrical approximation is required to find the bending shape of the crack. This is done by subdividing the crack edge into a number of straight segments defined by the gradient of the crack skeleton points. The detailed steps are as follows.

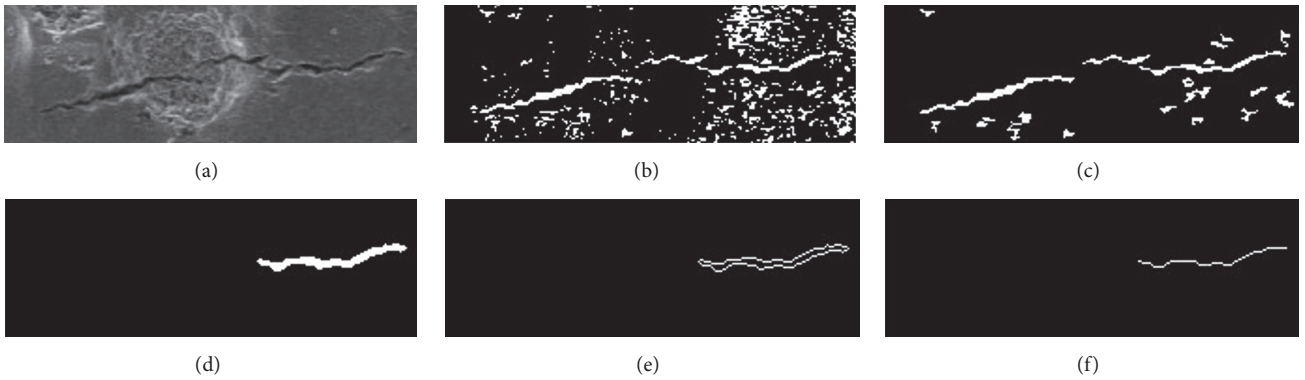

Figure 1: Real defect extraction. (a) Original image, (b) binary-conversion, (c) morphological processing, (d) cleaning processing, (e) edge obtaining, and (f) skeleton obtaining.

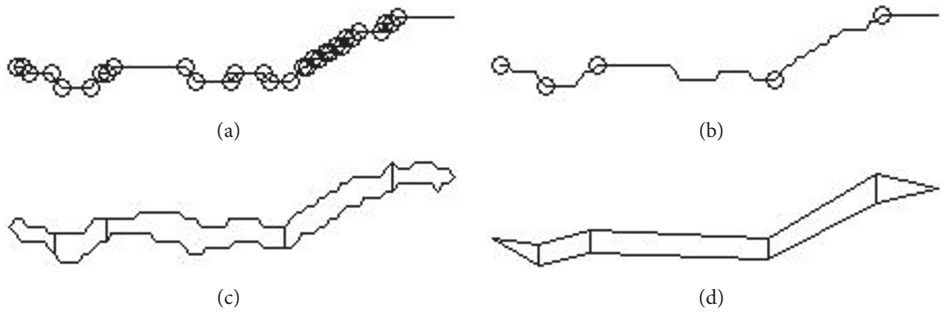

Figure 2: Defect model simplification. (a) Skeleton turning points, (b) subdivision points, (c) crack subdivision, and (d) crack linearization.

(a) It is assumed that i refers to the x coordinate of crack skeleton and $f(i)$ represents the y coordinate of it. Additionally, $f'(i) = \nabla f(i)$ presents the gradient of skeleton line and the large gradient stands for the segmentation of cracks. A threshold α is then defined. If the condition $f'(i) \geq \alpha$ is satisfied, the pixel i is counted as the turning point. Compute the gradient of each pixel in the skeleton line and store them in the set of $\psi(i)$. The skeleton turning points $\psi(i)$ are picked in terms of the slope changes of adjacent points. The results of the skeleton turning points are shown in Figure 2(a).

(b) Remove close skeleton turning points which satisfy the condition $\rho(\psi(i), \psi(j)) = \sqrt{(\psi_x(i) - \psi_x(j))^2 + (\psi_y(i) - \psi_y(j))^2} < \beta$ (ψ_x and ψ_y define coordinates of the pixels) to avoid unnecessary segmentations and screen out the proper ones (shown in Figure 2(b)).

(c) Take the screened skeleton turning points to divide the crack edge into several segments. It can be seen that the crack edge is divided into several connected crack segments in Figure 2(c). Each endpoint of segment is stored in the set of $\chi(i)$ and is called the boundary turning point.

(d) Since the boundaries of crack segments are irregular, it is necessary to build a simplified crack pattern approximating the original crack segment by straight lines. For each segment of the crack, connect boundary turning points $\chi(i)$ into straight lines and the edge of the original image can be changed into a series of line segment lists (shown in Figure 2(d)).

The overall simplified crack is presented as segments created by a set of straight lines forming a trapezoid space. It is easy to be parameterized to quantize the overall crack.

2.2.2. Model Parameterization. The damages of components are usually determined by the setting of defect positions and shapes. The changes of defect sizes, shapes, and positions can result in different weakening effects. Moreover, the damage degrees are different with different geometrical parameters. Thus, parameterization is applied for the future sensitive analysis.

For the tortuous crack, each crack segment is labeled by defined parameters, such as width, length, and orientation. Assume there are k ($k = 1, 2, \ldots, K$) boundary turning points stored in the vector of $\zeta(k) = (\zeta_x, \zeta_y)$ from small to large order of $\chi(k)$.

The parameters of the defect model include geometric parameters and position parameters, which are defined as follows.

(X, Y): the position (X, Y) is defined as the initial position of the crack tip, which is denoted as

$$X = \zeta_x(1) \tag{1}$$

$$Y = \zeta_y(1) \tag{2}$$

L: the length L is the average length of each crack segment n in the middle line, which is denoted as

$$L = \frac{2\sum_{n=1}^{K/2} L_n}{K} \tag{3}$$

where

$$L_n = \begin{cases} \dfrac{\sqrt{4\left(\zeta_x(2)-\zeta_x(1)\right)^2+\left(\zeta_y(3)+\zeta_y(2)-2\zeta_y(1)\right)^2}}{2} & n=1 \\ \dfrac{\sqrt{4\left(\zeta_x(K)-\zeta_x(K-1)\right)^2+\left(2\zeta_y(K)-\zeta_y(K-1)-\zeta_y(K-2)\right)^2}}{2} & n=\dfrac{K}{2} \\ \dfrac{\sqrt{4\left(\zeta_x(2n)-\zeta_x(2n-2)\right)^2+\left(\zeta_y(2n)+\zeta_y(2n+1)-\zeta_y(2n-1)-\zeta_y(2n-2)\right)^2}}{2} & others \end{cases} \tag{4}$$

W: the width W is the average width of each crack segment n in the vertical projection. Although the width of the actual crack groove may be more accurate, for the easy calculation, we choose the vertical coordinate difference, which does not have significant effect on the final result. W is denoted as

$$W = \frac{2\sum_{n=1}^{K/2-1}\left(\zeta_y(2n+1)-\zeta_y(2n)\right)}{K-2} \tag{5}$$

A: the angle A is defined as the average angle of connecting adjacent segments

$$A = \frac{2\sum_{n=1}^{K/2-1} A_n}{K-2} \tag{6}$$

where

$$\cos A_n = \begin{cases} \dfrac{4L_2^2+4L_1^2-4\left(\zeta_x(4)-\zeta_x(1)\right)^2-\left(\zeta_y(5)+\zeta_y(4)-2\zeta_y(1)\right)^2}{8L_2L_1} & n=1 \\ \dfrac{4L_{K/2}^2+4L_{K/2-1}^2-4\left(\zeta_x(K)-\zeta_x(K-3)\right)^2-\left(2\zeta_y(K)-\zeta_y(K-3)-\zeta_y(K-4)\right)^2}{8L_{K/2}L_{K/2-1}} & n=\dfrac{K}{2} \\ \dfrac{4L_n^2+4L_{n-1}^2-4\left(\zeta_x(2n+2)-\zeta_x(2n-2)\right)^2-\left(\zeta_y(2n+3)+\zeta_y(2n+2)-\zeta_y(2n-1)-\zeta_y(2n-2)\right)^2}{8L_nL_{n-1}} & others \end{cases} \tag{7}$$

D: the depth D of the crack is simplified to constant in order to exclude its impact on the structure based on the shape assumption [17, 22]. It is defined as

$$D = C \quad (C > 0) \tag{8}$$

in which C is a constant greater than 0 and smaller than the thickness of the blade.

3. Defect Model Sensitivity Analysis Optimization

The appearances of defects are random, and the lifecycles of different areas of the structure with defects are different. By discussing the parameters of the defect model, we can use the Sobol-based sensitivity analysis method to find the easily damaged area. Then in the next step, an optimization method can be adopted to strengthen this area to reduce the damage probability.

3.1. Sensitivity Selection Based on Sobol's Method. Parameters of the defect model have close relationship with structure damages. Since the crack may cause uneven stress distribution and concentrated stress, resulting in fracturing, we take the max equivalent stress as the evaluating indicator for sensitivity analysis. According to the geometric relations between crack and structure, the vulnerable area can be selected.

Figure 3 shows distributions of the equivalent stress in different conditions of the impeller blade. The impeller is constrained by the cylindrical coordinate in the axle hole with the inertial load of rotational angular velocity. It is shown in Figure 3 that the stress change is related to the crack location. Figure 3(a) indicates the stress distribution without crack, in which the value of maximum equivalent stress is 253.18MPa, and Figure 3(b) shows the stress distribution with crack in the nonfragile location, which shows that the maximum equivalent stress may not change a lot when the crack is not at the sensitive place. Figure 3(c) indicates that the maximum equivalent stress increases sharply to 414.15MPa when the crack is in the fragile location. It is shown that distributions of the equivalent stress change when the crack

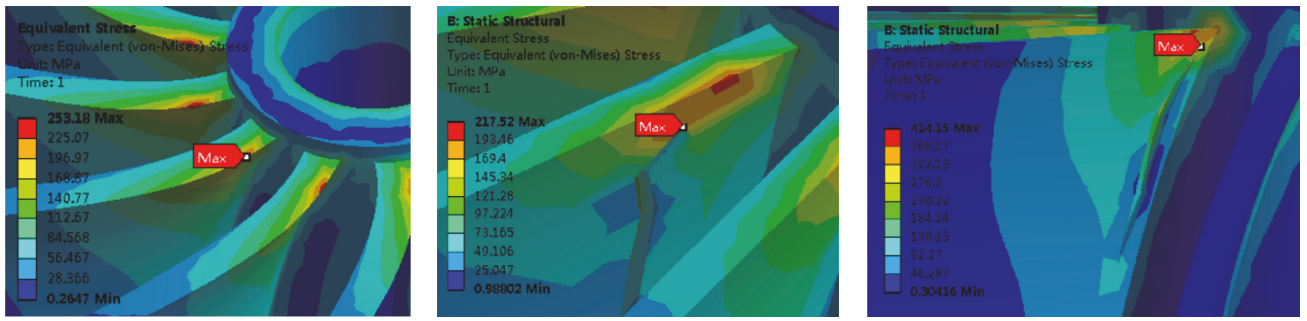

(a) (b) (c)

FIGURE 3: Stress distributions of the impeller blade. (a) Stress distribution without crack, (b) stress distribution with crack in the nonfragile location, and (c) stress distribution with crack in the fragile location (near the root of the impeller).

locations change. Thus, some areas may be vulnerable to the crack and the optimization of these areas is important for ensuring the safety of the component structure.

Sobol's method is a variance-based global sensitivity analysis technique that has been applied to computational models to assess the relative importance of input parameters on the output [23]. The usual Sobol sensitivity indices include the main and total effects for each input, but the method can also provide specific interaction terms, if desired. Based on Sobol's method, steps to obtain the parameter sensitivities of the half-real defect model are in the following.

(1) Sample defect model parameters twice independently with the sampling number n and make strength analysis. Denote output stress values as $f(x_1,x_2,x_3,x_4,x_5,x_6)$, $f(x_1, x_2', x_3', x_4', x_5', x_6')$, $f(x_1', x_2, x_3, x_4, x_5, x_6)$, $f(x_1', x_2, x_3', x_4', x_5, x_6')$, $f(x_1, x_2', x_3, x_4, x_5, x_6)$, $f(x_1', x_2', x_3, x_4', x_5', x_6')$, $f(x_1, x_2, x_3', x_4, x_5, x_6)$, $f(x_1', x_2', x_3', x_4, x_5', x_6')$, $f(x_1, x_2, x_3, x_4', x_5, x_6)$, $f(x_1', x_2', x_3', x_4', x_5, x_6')$, $f(x_1', x_2', x_3', x_4', x_5', x_6)$, and $f(x_1, x_2, x_3, x_4, x_5, x_6')$.

x is the position parameter for the first sampling, and x' is the parameter for the second sampling. x_1, x_2, x_3, and x_4 indicate parameters L, W, D, and A for the i^{th} segment, and x_5 and x_6 indicate parameters X and Y, respectively.

(2) Put equivalent stress values of the n groups in Sobol's function so that we can get the sensitivity value for each model parameter.

$$S_i = \frac{D_i}{D} \tag{9}$$

in which

$$D \approx \frac{1}{n}\sum_{m=1}^{n} f^2(x_m) - f_0^2 \tag{10}$$

$$D_i \approx \frac{1}{n}\sum_{m=1}^{n} f\left(x_{(\sim i)m}^{(1)}, x_{im}^{(1)}\right) f\left(x_{(\sim i)m}^{(2)}, x_{im}^{(1)}\right) - f_0^2 \tag{11}$$

$$D_{\sim i} \approx \frac{1}{n}\sum_{m=1}^{n} f\left(x_{(\sim i)m}^{(1)}, x_{im}^{(1)}\right) f\left(x_{(\sim i)m}^{(1)}, x_{im}^{(2)}\right) - f_0^2 \tag{12}$$

where x_{m} indicates the sampling points in the $\mathbf{I}^6$ space, and the superscripts (1) and (2) denote the $n \times 6$ sampling array of x.

Then the first-order sensitivity of the model parameter can be determined by $S_i = D_i/D$; the total sensitivity is determined by $S_{Ti} = 1 - D_{\sim i}/D$. The S_i shows the damage degree with the influence of the single parameter i, while S_{Ti} shows the damage degree with the influence of other parameters and i.

(3) Based on the value of S_{i}, sort model parameters and pick the larger one, which will cause a larger impact on the structure damage.

According to the sensitivity results, the most sensitive area and design parameters of the structure can be chosen as the optimized object. It provides selection basis for the next step.

3.2. Local Area Optimization. Generally, the structure design requires uniform stress distribution and less structure weight. For the structure with crack, the crack area usually has concentrated stress. Therefore, the objective function is formed as

$$\min F = [f_1, f_2] \tag{13}$$

where f_1 is the max equivalent stress, and f_2 is the structure weight. These two functions are affected by many parameters, and these parameters are different for different mechanical elements. Given a specific element, according to the results of sensitivity analysis, we can select the corresponding structural parameters for optimization, and we will take the impeller blade for example in the experimental section and introduce it in detail later.

Thus, steps for local area optimization are as follows.

(1) The defect model parameters with high sensitivity are determined according to Sobol's sensitivity results.

(2) Sampling is carried out according to the variation range of the determined parameters, and the output value of each sampling point is analyzed.

(3) Based on the SVM method, the prediction model of optimization variables and optimization goal can be formed (Mech, 2015). The SVM algorithm consists of the

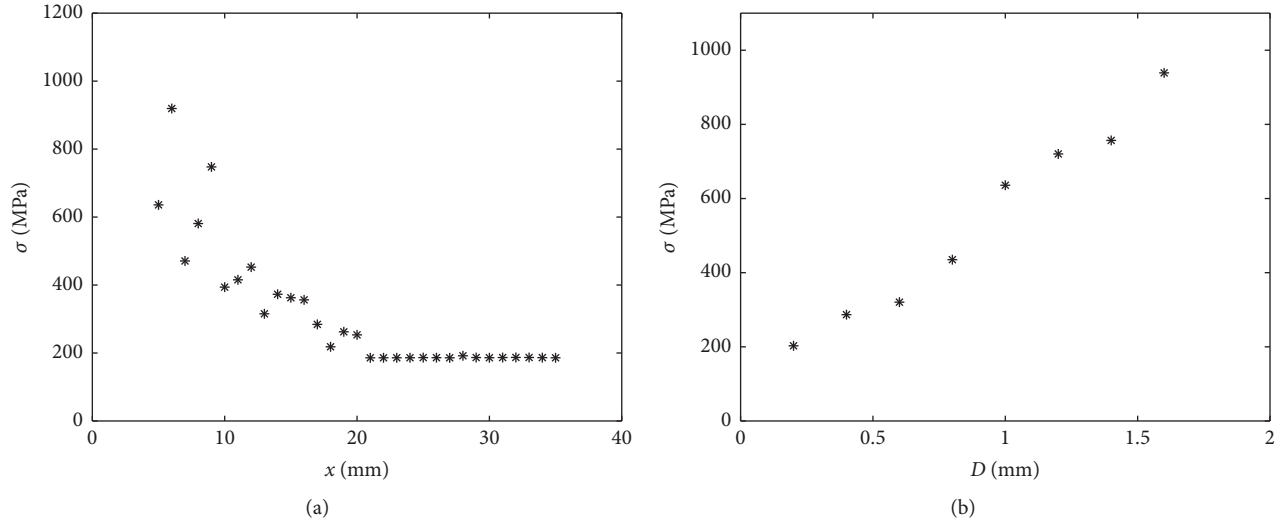

Figure 4: The relationship between parameters with large sensitivity and the maximum equivalent stress σ. (a) In the situation of X. (b) In the situation of D.

following steps. (1) The input space is transformed into a high-dimensional space by nonlinear transformation, which is realized by defining an appropriate inner product kernel function. (2) Solve convex quadratic programming problem under the condition of maximizing interval. (3) Find the optimal classification surface in the new space, which is the maximum interval classification surface.

(4) The PSO method is adopted finally to determine the optimal solution set [24] . The PSO algorithm consists of three steps: (1) Evaluate fitness of each particle and each evaluation solution is represented by a particle in the fitness landscape (search space). (2) Update individual and global best values. (3) Update velocity and position of each particle, which are based on some parameters: inertial coefficient and acceleration coefficients and individual best solution of both particle and swarm. These steps are repeated until the results of two adjacent iterations are similar.

4. Example with the Impeller Blade

4.1. Model Validation. Impeller is the main bearing part of the compressor. It stands various alternating stress and has a very bad working condition. Therefore, cracks often appear which will result in fatigue fracture of impeller and can cause damage to the people and equipment around.

Thus, in this paper, we take the impeller blade as the research subject to verify the validity of the proposed method. Since blade is thin and the probability of occurrence of deep cracks is low, we only discuss the influence of the surface crack. We choose the root of the impeller entry end as the reference point of the crack mode. By sampling the model parameters twice with the sampling number 100, we can obtain sensitivity analysis results for the maximum equivalent stress in Table 1.

The absolute value in the sensitivity result indicates the sensitivity of the input parameters to the output. The vulnerable area can be picked according to the parameters

Table 1: The sensitivity analysis results for the maximum equivalent stress.

Sensitivity	S	S_T
L	9.1	2.6
W	10.7	-3.6
D	58.8	2.2
A	5.6	1.2
X	44.3	-9.9
Y	5.2	-9.8

which have larger sensitivity values. In Table 1, S is the first-order sensitivity which indicates the effect of this single parameter on the results, and S_T is the total sensitivity which shows the effect of this parameter and other ones. It can be seen that model parameters D and X have larger values of S, and none of parameters has large value of S_T. The results showed that the depth and the horizontal position have larger influence on the blade damage. For these two parameters, we discuss their relationships with the maximum equivalent stress in Figure 4.

Figure 4(a) indicates the relationship between X and σ, and Figure 4(b) indicates the relationship between D and σ. From Figure 4(a), it is shown that the stress is enhanced with the crack location being closer to the blade root. Meanwhile, when the parameter X is larger than 20, the stress value remains stable. According to this result, the area near the blade root is easy to be damaged by cracks. This easily damaged area is needed to be strengthened to resist fatigue fracture; so we take the blade root as the optimization area. From Figure 4(b), stress increases with the increase of crack depth. According to the corresponding relationship between the crack depth and the blade thickness, we choose the blade thickness of the blade root as the optimization object to thicken the blade root area.

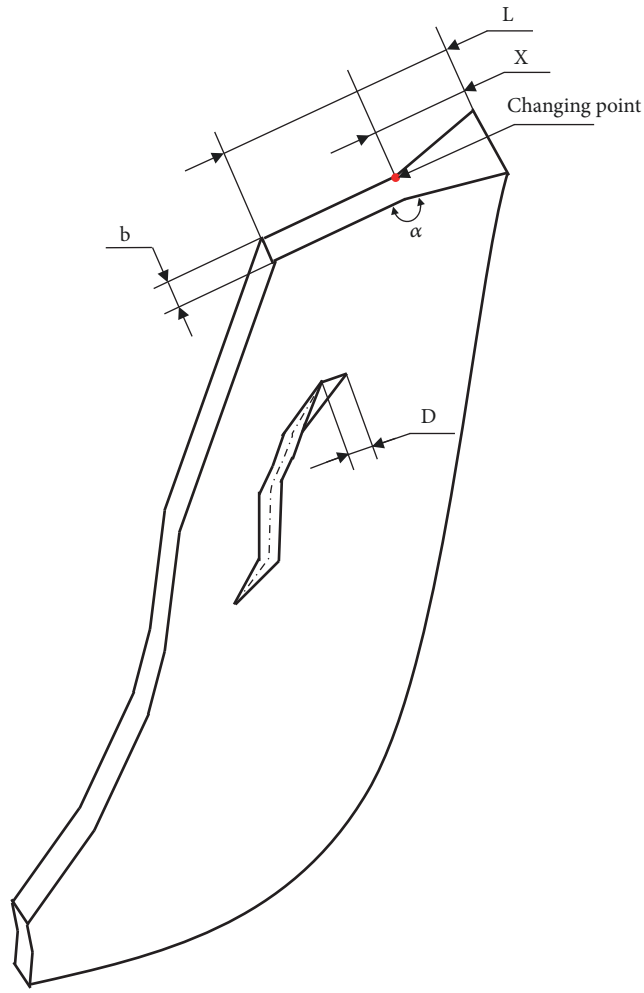

Figure 5: Relationship between crack parameters and optimization variables.

Figure 5 shows the relationship between crack parameters and optimization variables in the impeller blade. The changing point is determined by X and α (angle of thickening area) and b represents blade thickness away from root. It is known that the parameters X and D of impeller have a great influence on the blade. In order to improve the reliability of impeller, it is necessary to optimize the blade structure to enhance the resistance of the blade to these two parameters. The resistance of blade to cracks increases when the ratio D/b gets smaller. In the same way, the blade's resistance to cracks can also be enhanced when root thickness is designed larger as the root is more sensitive to cracks. Obviously, the values of X and α determine the thickness of the root. When the other optimization parameter remains unchanged, the large value of X and the small value of α both cause the increase of root thickness.

4.2. Optimization Process. The changing position and the angle of the thickening area are chosen as optimization variables, and maximum equivalent stress and structure weight are simultaneously set as the optimization goal. Thus, the objective function is formed as

$$\begin{aligned} \min \quad & \underset{b,\alpha,X}{F} = [f_1, f_2] \\ s.t. \quad & b > 0 \\ & 90^\circ < \alpha < 180^\circ \\ & 0 < X < L \end{aligned} \tag{14}$$

where f_1 is the max equivalent stress, and f_2 is the structure weight. b is the blade thickness, α is the angle of thickening area, X is the changing position of thickening area from the root, and L is the length of the blade.

We sampled the optimization variables to obtain 300 sets of sample points. The 230 groups of sample points are selected for training, and 70 groups are used for testing. We used the RBF (Basis Function Radial) kernel function in the SVM prediction model. By using the cross validation method, the best parameter can be searched. The prediction results are shown in Figure 6.

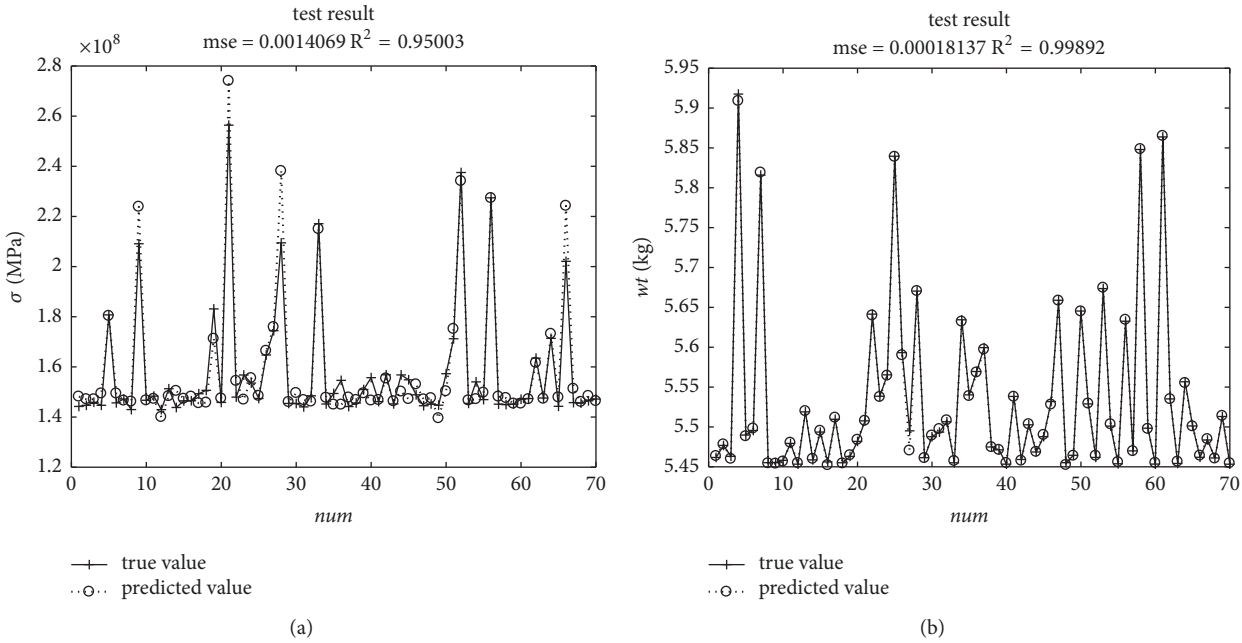

Figure 6: The prediction results based on SVM. (a) The result of the maximum equivalent stress σ. (b) The result of the structure weight wt.

It can be seen that the mean square error MSE and the decision coefficient R2 in the testing results all meet the requirements, which means the prediction effect is good. We also compared this result with the response surface method and the BP neural network method based on the same sample groups. The response surface method uses quadratic polynomial to establish the forecasting model. The comparison results are shown in Table 2.

It is shown that the SVM prediction model has higher precision value and can better establish the mapping relationship between the optimization variables and the optimization goal. Thus, SVM is chosen as the prediction model for the subsequent structural optimization.

Based on the SVM, we optimize the sensitive area for the impeller blade according to the selected optimization variables and optimization goal.

In the particle swarm optimization algorithm, we set c_1=1.2 and c_2=1.2. The population size is 200, the number of iteration is 500, and the weight coefficient is set as $\omega_{\min} = 0.1$ and $\omega_{\max} = 1.2$. The distribution of the Pareto solution set is obtained as shown in Figure 7 and Table 3. The final plan can be selected according to the preference of the optimization object.

By considering both of the safety and the cost, the maximum equivalent stress and the weight have equal weighting factor. Thus, the optimal solution is plan 7. The optimal variation angle is 173.26° and the optimal variation position is 27.37 mm. Before optimization, the thickness of blade was 20.00mm. Thus, the change of thickness is 7.37mm and the change of angle is 6.74°.

Using the optimization result discussed above, the blade structure can be strengthened. To verify the effectiveness of the proposed optimization method, we placed a crack on the vulnerable root area of the blade and analyzed the strength of the structure. The crack depth is set as D=1mm and its position parameters are set as X=5mm and Y=1mm. We also compared the proposed method with other two methods in Shi et al. [26] and Wang [25]. Wang [25] used the equal thickness to avoid structure fatigue. The thickness has a gradual change from the root to the tip in Shi et al. [26]. The comparison analysis results are shown Figure 8.

Table 2: The comparison results by using different prediction models.

Method	MSE	R2
SVM	0.0014069	0.95003
BP neural network	0.0022762	0.93924
Response surface	26.9243	0.5442

Figure 8(a) is the analysis result before optimization. Figure 8(b) is the result after optimization by using the proposed method. Figures 8(c) and 8(d) are results by using the optimization methods mentioned in Wang [25] and Shi et al. [26]. It is shown that the three optimization methods can reduce the maximum equivalent stress more or less. However, the two compared methods ignore the defect factors during the optimization process. They only improve the distribution of stress based on the analysis of the defect-free structure. Although the stress value can be reduced accordingly, the maximum equivalent stress is still concentrated in the area of crack, which means that the crack will grow rapidly and cause the early scrap of the impeller easily. The proposed

Table 3: Pareto solution set.

Plan	Variation angle/(°)	Variation position/mm	Maximum equivalent stress /MPa	Weight/kg
1	172.30	26.22	145.7021	5.4756
2	172.56	29.27	145.1803	5.4927
3	172.43	32.32	145.9901	5.5177
4	172.86	31.94	145.1191	5.5113
5	173.11	25.23	156.7075	5.4692
6	173.00	24.01	156.8309	5.4649
7	173.26	27.37	146.2355	5.4786
8	171.90	30.79	147.4149	5.5079
9	171.72	24.24	157.3187	5.4676
10	173.18	31.02	145.1802	5.5018
11	172.64	32.93	145.5296	5.5216
12	171.82	30.34	145.6820	5.5045
13	171.78	23.02	158.8557	5.4631

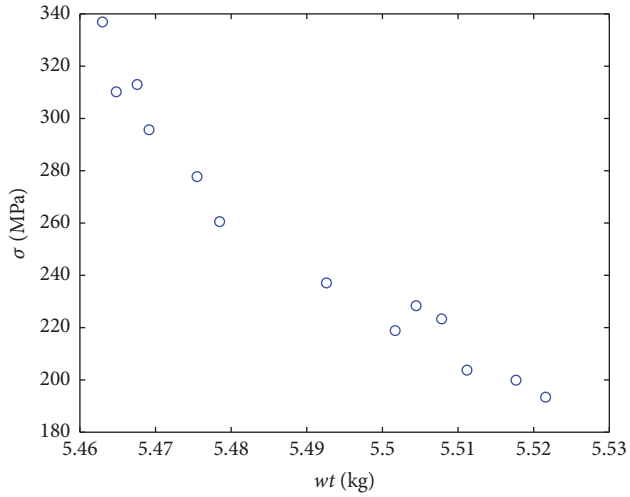

Figure 7: Distributions of the Pareto solution set.

method optimizes structure directly from the view of anti-defect method. It can both increase impeller strength and avoid the stress concentration.

We also record the weight and the max equivalent stress value of the comparison methods in Table 4. After the optimization, the weight of the impeller is 5.4832 kg and the max equivalent stress of the proposed method is 146.86 MPa. It can be seen that the increase of weight is the smallest and the decrease of stress is the largest. Compared to the other two methods, the proposed method has the best optimization results. Furthermore, the structure strength is enhanced well and the max equivalent stress is not concentrated in the crack region. Thus, based on the proposed method, the impeller can have a certain resistance to defect so that the weakening effect of the defect can be delayed.

Besides the max stress and weight, the flow field is another main factor that may be influenced after the optimization. However, due to the uniform thickness of the optimized impeller blades in the axial direction, the cross-section of the flow path formed by the impeller blades has the same trend and thus does not affect the impeller performance.

5. Conclusion

For mechanical elements running under severe working condition, there inevitably exist small defects. The weak areas are more affected, resulting in early damage during service. Thus, a novel anti-defect optimization method based on half-real defect model and Sobol's sensitivity is proposed to decrease the weakening effect of defects. Finally, we take the impeller blade, for example, to test the effectiveness of the proposed method. From the results we can conclude the following.

(1) A half-real defect model was built on the basis of the plane characteristics of the defect image. Influences of geometrical and location parameters of the defect model are analyzed for the defect-resisting performance. The model

Table 4: The comparison results of the three methods.

	Before optimization	After optimization using Wang [25]	After optimization using Shi [26]	After optimization using the proposed
Weight /kg	5.4543	6.07	5.7536	5.4842
Max stress /MPa	217.52	187.99	192.16	146.86
Max stress region	crack region	crack region	crack region	other region

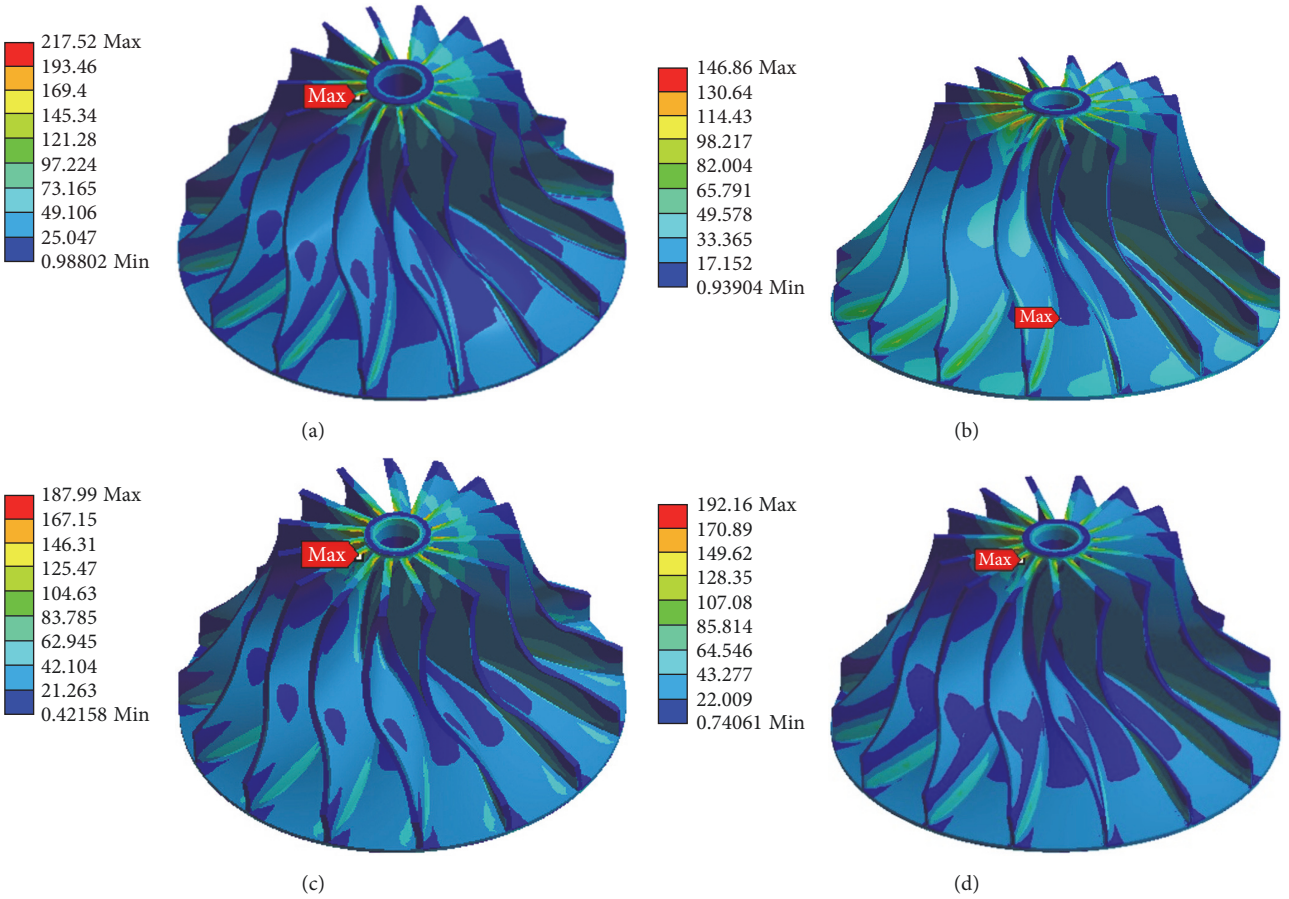

Figure 8: Stress comparison results. (a) The analysis result before optimization. (b) The result after optimization using the proposed method. (c) The result after optimization using Wang [25]. (d) The result after optimization using Shi et al. [26].

parameters can possibly play an effective role in the simulation of the weakening effect on structure.

(2) The weakness of the structure was analyzed combining Sobol's sensitivity method. The optimization area and optimization variables are selected pertinently according to the parameters with high sensitivity. Based on the PSO algorithm, the weakening effect of defects on the structure can be decreased effectively.

Data Availability

All data included in this study are available upon request from the corresponding author.

Conflicts of Interest

The authors declare that there are no conflicts of interest.

Acknowledgments

This research was supported by National Key R&D Program of China (2018YFB1700504), NSFC (51775498, 51775497), and ZPNSFC (LY17F030011).

References

[1] G. Ananthasuresh K, *A nEw Design Paradigm for Micro-Electro-Mechanical Systems and Investigations on the Compliant*

Mechanism Synthesis [Ph.D. thesis], University of Michigan, Ann Arbor, Mich, USA, 1994.

[2] B. Zhu, X. Zhang, and S. Fatikow, "Structural topology and shape optimization using a level set method with distance-suppression scheme," *Computer Methods in Applied Mechanics & Engineering*, vol. 283, pp. 1214–1239, 2015.

[3] Q. Xia, T. Shi, S. Liu, and M. Y. Wang, "Shape and topology optimization for tailoring stress in a local region to enhance performance of piezoresistive sensors," *Computers & Structures*, vol. 114-115, no. 1, pp. 98–105, 2013.

[4] G. Han, Y. Chen, and X. Wang, "Flutter analysis of bending–torsion coupling of aero-engine compressor blade with assembled clearance," *Applied Mathematical Modelling*, vol. 39, no. 9, pp. 2539–2553, 2015.

[5] C. W. Fei, W. Z. Tang, and G. C. Bai, "Novel method and model for dynamic reliability optimal design of turbine blade deformation," *Aerospace Science & Technology*, vol. 39, pp. 588–595, 2014.

[6] A. Staino and B. Basu, "Dynamics and control of vibrations in wind turbines with variable rotor speed," *Engineering Structures*, vol. 56, no. 6, pp. 58–67, 2013.

[7] L. Li, Y. H. Li, Q. K. Liu, and H. W. Lv, "A mathematical model for horizontal axis wind turbine blades," *Applied Mathematical Modelling*, vol. 38, no. 11-12, pp. 2695–2715, 2014.

[8] J. Hong, B. Li, Y. Chen, and H. Peng, "Study on the optimal design of engine cylinder head by parametric structure characterization with weight distribution criterion," *Journal of Mechanical Science & Technology*, vol. 25, no. 10, p. 2607, 2011.

[9] M. Islam, A. Buijk, M. Rais-Rohani, and K. Motoyama, "Simulation-based numerical optimization of arc welding process for reduced distortion in welded structures," *Finite Elements in Analysis & Design*, vol. 84, no. 1, pp. 54–64, 2014.

[10] Y. Liu, L. Tan, and S. L. Cao, "The micro genetic algorithm and its usage in the optimization design of mixed-flow pump," *Machinery Design & Manufacture*, vol. 9, pp. 1–3, 2012 (Chinese).

[11] W. Song, A. Keane, J. Rees, A. Bhaskar, and S. Bagnall, "Turbine blade fir-tree root design optimisation using intelligent CAD and finite element analysis," *Computers & Structures*, vol. 80, no. 24, pp. 1853–1867, 2002.

[12] J. Chen, Q. Wang, W. Z. Shen, X. Pang, S. Li, and X. Guo, "Structural optimization study of composite wind turbine blade," *Materials & Design*, vol. 46, no. 4, pp. 247–255, 2013.

[13] V. N. Shlyannikov, R. R. Yarullin, and A. P. Zakharov, "Fatigue of steam turbine blades with damage on the leading edge," in *Proceedings of the European Conference on Fracture*, vol. 3, pp. 1792–1797, 2014.

[14] N. Ejaz and A. Tauqir, "Failure due to structural degradation in turbine blades," *Engineering Failure Analysis*, vol. 13, no. 3, pp. 452–463, 2006.

[15] S. M. Clarke, J. H. Griebsch, and T. W. Simpson, "Analysis of support vector regression for approximation of complex engineering analyses," in *Proceedings of the ASME 2003 International Design Engineering Technical Conferences and Computers and Information in Engineering Conference*, vol. 127, pp. 1077–1087, American Society of Mechanical Engineers, 2005.

[16] Y. Shi, "Particle swarm optimization: developments, applications and resources," in *Proceedings of the 2001 Congress on Evolutionary Computation*, vol. 1, pp. 81–86, IEEE, 2001.

[17] J. G. Wu, *Theoretical and Applied Research on Crack Growth and Damage Evolution [Ph.D. thesis]*, Beijing University of Aeronautics and Astronautics, 2009.

[18] J. M. Yin, X. Y. Zhao, and S. Y. Zhang, "Method for designing parts structure to resist harsh environments considering sobol defects sensitivity," *Journal of Zhejiang University (Engineering Science)*, vol. 49, no. 8, pp. 1487–1494, 2015 (Chinese).

[19] W. Withayachumnankul, P. Kunakornvong, C. Asavathongkul, and P. Sooraksa, "Rapid detection of hairline cracks on the surface of piezoelectric ceramics," *The International Journal of Advanced Manufacturing Technology*, vol. 64, no. 9-12, pp. 1275–1283, 2013.

[20] B. Y. Lee, Y. Y. Kim, S.-T. Yi, and J.-K. Kim, "Automated image processing technique for detecting and analysing concrete surface cracks," *Structure and Infrastructure Engineering*, vol. 9, no. 6, pp. 567–577, 2013.

[21] R. S. Adhikari, O. Moselhi, and A. Bagchi, "Image-based retrieval of concrete crack properties for bridge inspection," *Automation in Construction*, vol. 39, pp. 180–194, 2014.

[22] A. Saito, M. P. Castanier, and C. Pierre, "Estimation and veering analysis of nonlinear resonant frequencies of cracked plates," *Journal of Sound & Vibration*, vol. 326, no. 3, pp. 725–739, 2009.

[23] I. M. Sobol, "Sensitivity estimates for nonlinear mathematical models," *Mathematical Modelling and Computational Experiment*, vol. 1, no. 1, pp. 112–118, 1993.

[24] E. Zahara and Y.-T. Kao, "Hybrid Nelder-Mead simplex search and particle swarm optimization for constrained engineering design problems," *Expert Systems with Applications*, vol. 36, no. 2, pp. 3880–3886, 2009.

[25] S. X. Wang, *Semi-Closed Pump Impeller*, China, 2014.

[26] Y. Q. Shi, W. M. Wang, and X. Ning, *Development of Parameterized Design Programme for Centrifugal Compressor T Type Impeller*, Compressor Blower & Fan Technology, 2012.